Aqua-Mediated Hydrothermal Synthesis in the Production of a g-C$_3$N$_4$/TiO$_2$ Composite for Photocatalytic Degradation of RR4 Dye

Nur Aien Muhamad[1], Muhamad Afiq Rosli[1], Siti Raihan Hamzah[1], Nureel Imanina Abdul Ghani[1], Nadiah Sabihah Md Natar[1], Mohammad Saifulddin Mohd Azami[1], Mohd Azlan Mohd Ishak[1], Sumiyyah Sabar[2] and Wan Izhan Nawawi Wan Ismail[1]*

[1]Faculty of Applied Science, Universiti Teknologi MARA, 02600 Arau, Perlis, Malaysia
[2]School of Distance Education, Universiti Sains Malaysia, 11800 Minden, Pulau Pinang, Malaysia
*Corresponding author (e-mail: wi_nawawi@uitm.edu.my)

The synthesis of a composite material comprising g-C$_3$N$_4$ and TiO$_2$ was effectively achieved through successful sol-gel and hydrothermal techniques, utilizing water as the solvent. The fabrication process involved employing a titanium (IV) butoxide precursor for TiO$_2$ formation, while production of g-C$_3$N$_4$ involved the thermal polymerization of urea. In comparison to both synthesized TiO$_2$ and g-C$_3$N$_4$, the g-C$_3$N$_4$/TiO$_2$ composite performed better under visible light irradiation where it showed outstanding photocatalytic activity using RR4 dye as a model pollutant. 5 % of g-C$_3$N$_4$ composited into TiO$_2$, denoted as TCN$_5$, demonstrated superior performance, exhibiting an optimal rate constant (k) of 0.0920 min^{-1} when degrading 30 mg L^{-1} RR4 dye within 1 hour under a 55 W fluorescent lamp. The degradation percentage increased to 99.73%, indicating an improvement that was twice that of TiO$_2$ and four times greater than that of g-C$_3$N$_4$ alone. The synthesized g-C$_3$N$_4$/TiO$_2$ was further studied using a range of analytical techniques, including X-ray diffraction (XRD), Fourier Transform infrared (FTIR), field-emission scanning electron microscopy with energy dispersive X-ray (FESEM-EDX), elemental mapping analysis, and UV-visible diffuse reflectance spectroscopy (UV-DRS), to confirm its structural and optical properties.

Keywords: Photocatalysis; graphitic carbon nitride; titanium dioxide; RR4 dye

The textile sector is a major consumer of dyes and holds a pivotal position in worldwide dye production. Dyes are indispensable within the textile industry since they enhance a fabric's visual appeal by imparting colour to it. Nevertheless, the textile manufacturing process generates wastewater containing dyes, giving rise to substantial environmental and public health issues. Additionally, industrial operations and other sources contribute to the release of wastewater that may contain a range of organic contaminants, including dyes [1]. These organic substances are responsible for adding colour to a range of materials such as paper, plastic, textiles and leather. The manufacturing process of these materials generates wastewater containing organic pollutants such as dyes. Treating dye wastewater poses a significant challenge due to the intricate and resilient nature of dyes, which makes them difficult to break down using traditional treatment methods such as biological treatment, chemical oxidation, and physical adsorption [2]. As a result, there is an increasing interest in creating innovative and efficient treatment methods for dye wastewater, with photocatalysis being one of the highly anticipated technologies in this area. Photocatalysis is a chemical process that involves the utilization of a photocatalyst, typically a semiconductor material like zinc oxide (ZnO) [3], titanium dioxide (TiO$_2$) [4], or cadmium sulfide (CdS) [5], among others, to accelerate a reaction in the presence of light to degrade organic dyes. Out of all the photocatalysts available, TiO$_2$ has been identified as one of the most effective semiconductors.

TiO$_2$ is a semiconductor material that is particularly noteworthy due to its many advantages, including low cost, chemical and biological stability, and strong photocatalytic properties. It has the potential to be very useful in wastewater treatment as well as in other applications, such as self-cleaning surfaces and air purification [6]. When exposed to light, TiO$_2$ can cause organic compounds to decompose as a result of activated electrons and holes. Despite its effectiveness as a photocatalyst, TiO$_2$ has drawbacks, one of which is its limited ability to harness solar energy for photocatalytic reactions due to its bandgap, which is relatively large (~3.2 eV) [7]. As a result, TiO$_2$ can only absorb a small amount of the solar spectrum, particularly in the ultraviolet region, which restricts its photocatalytic activity to UV light. UV light accounts for only approximately 5% of the total solar spectrum. Another drawback of TiO$_2$ is its vulnerability to photo-corrosion, which can gradually diminish its photocatalytic performance. When exposed

111 Nur Aien Muhamad, Muhamad Afiq Rosli, Siti Raihan Hamzah,
Nureel Imanina Abdul Ghani, Nadiah Sabihah Md Natar,
Mohammad Saifulddin Mohd Azami, Mohd Azlan Mohd
Ishak, Sumiyyah Sabar and Wan Izhan Nawawi Wan Ismail

Aqua-Mediated Hydrothermal Synthesis in
the Production of a g-C$_3$N$_4$/TiO$_2$ Composite
for Photocatalytic Degradation of RR4 Dye

to light, TiO$_2$ can produce electron-hole pairs that interact with water molecules to create reactive oxygen species. These species can subsequently corrode the TiO$_2$ surface, leading to a reduction in surface quality and decreased photocatalytic performance. To address the limitations of TiO$_2$, it is necessary to create novel materials and modify existing ones to enhance its photocatalytic performance and broaden its light absorption spectrum beyond the UV region. Previous studies have attempted modifying TiO$_2$ to improve its photocatalytic activity. Various techniques have been employed, such as metal doping [8], non-metal doping [9], and co-catalyst deposition [10]. However, recent research has focused on the use of g-C$_3$N$_4$, which has shown promising results when combined with TiO$_2$, and several studies have demonstrated its superior performance and efficiency.

In our investigation, we synthesized a g-C$_3$N$_4$/ TiO$_2$ composite using a combination of sol-gel and hydrothermal techniques, with water as the solvent. It is important to point out that the hydrothermal method is recognized for its ability to enhance photocatalytic activity through the formation of a photocatalyst with a high specific surface area [18]. This composite, containing 5 wt.% g-C$_3$N$_4$, demonstrated remarkable photocatalytic efficiency under visible light exposure, particularly in the degradation of RR4 dye. Furthermore, we conducted a thorough analysis to explore the physical phase composition, surface properties, and optical characteristics of the composite. In summary, the g-C$_3$N$_4$/TiO$_2$ photocatalyst exhibited exceptional photocatalytic performance.

EXPERIMENTAL

Chemicals and Materials

Titanium (IV) butoxide (Ti(C$_4$H$_9$O)$_4$) (Pur. 97%), urea (CO(NH$_2$)$_2$, Pur. 99%), and Reactive Red 4(RR4) dye, used as a model pollutant, were all purchased from Sigma Aldrich. Distilled (DI) water was used as the solvent throughout this study.

Synthesis of g-C$_3$N$_4$

The g-C$_3$N$_4$ powder was generated through the thermal polymerization of urea. Initially, 20 g of urea powder were placed inside a closed crucible. Subsequently, the powder was subjected to calcination in a muffle furnace, at a temperature of 550 °C for 30 minutes, with a gradual heating rate of 3 °C/min. After cooling to room temperature, a pale yellow solid form of g-C$_3$N$_4$ was produced.

Synthesis of g-C$_3$N$_4$/TiO$_2$

A composite material comprising g-C$_3$N$_4$ and TiO$_2$ was synthesized through a combination of the sol-gel method and a hydrothermal process, as shown in **Figure 1**. Initially, 1 % by weight of g-C$_3$N$_4$ was blended with 7.5 mL of distilled water and agitated for 15 minutes. Subsequently, 7.5 mL of titanium (IV) butoxide was introduced into the mixture and stirred for 2 hours in an ice bath. The resulting solution underwent hydrothermal treatment at 180 ºC for a duration of 4 hours. The resultant sample was then subjected to drying at 100 ºC and calcination for 2 hours at 550 ºC. Depending on the mass ratio of g-C$_3$N$_4$ with TiO$_2$ (1 %, 2 %, 5 %, and 10 %), the composite materials were labelled TCN$_1$, TCN$_2$, TCN$_5$, and TCN$_{10}$, respectively. To facilitate a comparative analysis, the same procedure was employed to fabricate TiO$_2$ without the inclusion of g-C$_3$N$_4$.

Photocatalytic Degradation of RR4 Dye

The photocatalytic performance of the prepared samples was assessed by measuring the absorption of an RR4 dye solution in the presence of TCN$_X$. A 55-watt light bulb was utilized as the light source and positioned 5 cm above a petri dish. 0.025 grams of the synthesized sample was dissolved in 30 mL of a 30 mg L^{-1} RR4 dye solution through ultrasonic treatment. At 15-minute intervals, 4 mL of the solution was extracted to determine the degradation efficiency of the photocatalyst under UV-Visible light at a wavelength of 517 nm, using a HACH DR1900 spectrophotometer.
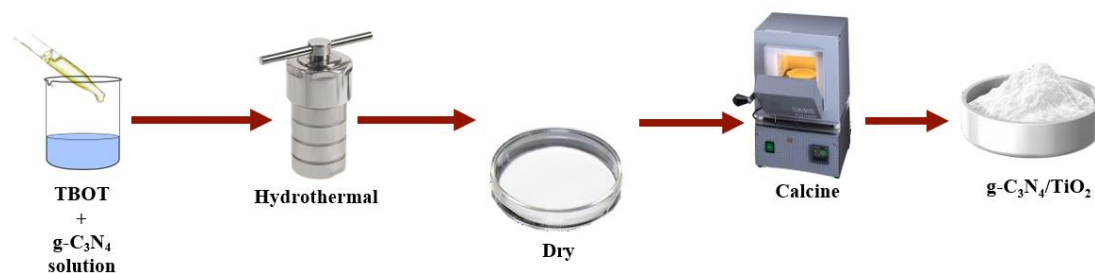

Figure 1. Synthesis process of the photocatalyst, g-C$_3$N$_4$/TiO$_2$

112 Nur Aien Muhamad, Muhamad Afiq Rosli, Siti Raihan Hamzah, Nureel Imanina Abdul Ghani, Nadiah Sabihah Md Natar, Mohammad Saifulddin Mohd Azami, Mohd Azlan Mohd Ishak, Sumiyyah Sabar and Wan Izhan Nawawi Wan Ismail

Aqua-Mediated Hydrothermal Synthesis in the Production of a g-C₃N₄/TiO₂ Composite for Photocatalytic Degradation of RR4 Dye
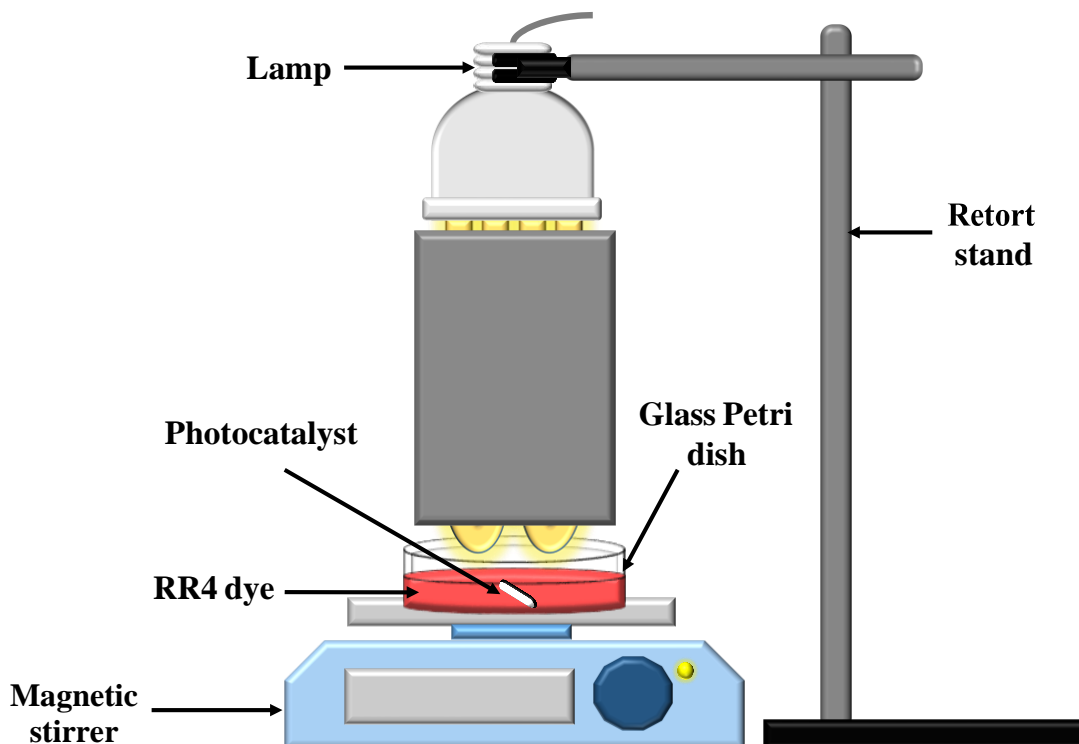
Figure 2. Experimental setup for the photocatalytic degradation of RR4 dye.

Characterization Study

Various analytical techniques were employed to investigate the synthesized samples of TiO_2, $g\text{-}C_3N_4$, and TCN_X. The crystallinity of the composite samples was assessed with X-ray diffraction (XRD) analysis, using a Bruker D8 Advance diffractometer. To identify the functional groups within the samples, Fourier Transform Infrared-Attenuated Total Reflectance (FTIR-ATR) analysis was carried out using a Perkin-Elmer model 2000 FTIR analyzer. The surface characteristics of the samples were examined using a Field Emission Scanning Electron Microscope (SEM) analyzer, specifically the LEO SUPRA 50 VP Field Emission SEM. Additionally, an elemental composition analysis was performed using EDX spectroscopy and elemental mapping. The bandgap energy of the synthesized sample was determined using Ultraviolet Visible-Diffuse Reflectance Spectroscopy (DRS) with a Perkin Elmer Lambda 35 instrument, covering a wavelength range from 200 to 800 nm.

RESULTS AND DISCUSSION

Characterization of g-C₃N₄/TiO₂

The XRD patterns of $g\text{-}C_3N_4$, TiO_2, and TCN_X, with varying amounts of composite $g\text{-}C_3N_4$ (X = 1 %, 2 %, 5 % and 10 %) are presented in **Figure 3**. Two distinctive peaks are evident at 13.1° and 27.6 °, corresponding to the (100) and (002) crystalline planes of $g\text{-}C_3N_4$, as documented in JCPDS 01-087-1526. The (100) peak signifies s-triazine, while the (200) peak signifies the $g\text{-}C_3N_4$ aromatic system [19]. For pure TiO_2, several peaks are visible at 25.61° (101), 38.07 ° (004), 48.34 ° (200), 54.14 ° (105), 55.36 ° (211), and 63.7 ° (213), consistent with the TiO_2 anatase phase. **Figure 3** shows that the $g\text{-}C_3N_4$ peak is not visible in the TCN_X photocatalyst, leaving only the TiO_2 peak. According to the Matias et al, the $g\text{-}C_3N_4$ peak may not be detected due to the relatively limited amount of $g\text{-}C_3N_4$ integrated into the TiO_2 composite [20].

113 Nur Aien Muhamad, Muhamad Afiq Rosli, Siti Raihan Hamzah,
Nureel Imanina Abdul Ghani, Nadiah Sabihah Md Natar,
Mohammad Saifulddin Mohd Azami, Mohd Azlan Mohd
Ishak, Sumiyyah Sabar and Wan Izhan Nawawi Wan Ismail

Aqua-Mediated Hydrothermal Synthesis in
the Production of a g-C$_3$N$_4$/TiO$_2$ Composite
for Photocatalytic Degradation of RR4 Dye
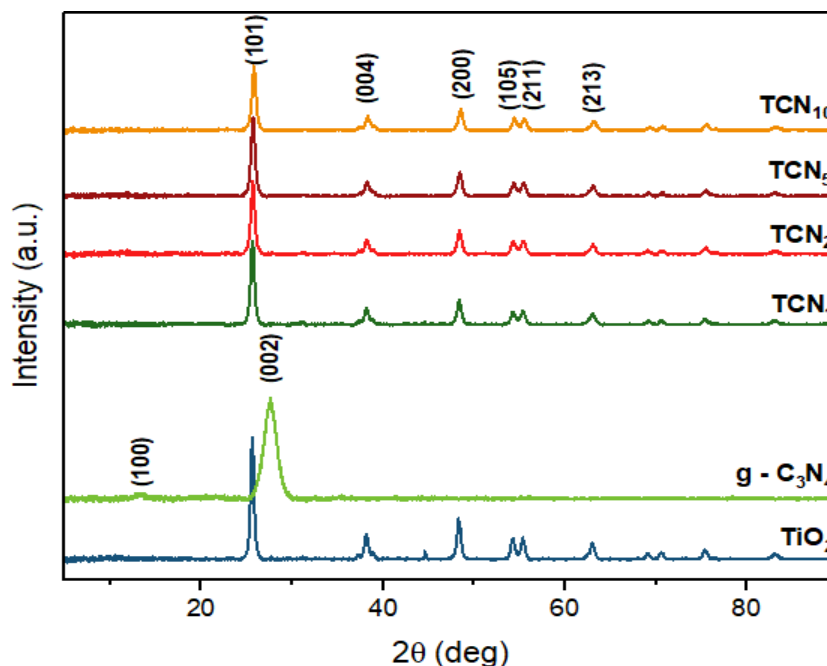
Figure 3. XRD spectra of TiO$_2$, g – C$_3$N$_4$, TCN$_1$, TCN$_2$, TCN$_5$ and TCN$_{10}$.

XRD analysis provides valuable insights into the synthesized sample, including details about the crystallite size, which can be determined using the Scherrer equation, as presented below. The Scherrer equation is utilized to ascertain the size of the crystallite (L) in the synthesized sample. This equation takes into account the radiation wavelength (λ), which is determined from XRD, as well as the full width at half maximum (FWHM) of peaks (β) expressed in radians at any 2θ position within the pattern [21]. To compute the crystallite size for TiO$_2$, g-C$_3$N$_4$, TCN$_1$, TCN$_2$, TCN$_5$, and TCN$_{10}$, Eqn. 1 is applied. The calculated sizes of the crystallites, along with their respective crystallinity percentages, are presented in Table 1.

As indicated in Table 1, the TCN$_5$ photocatalyst exhibited the highest crystallite size and crystallinity index among all the samples, at 6.97 nm and 72.62 %, respectively. Among the various samples, it is evident that the incorporation of 5 % g-C$_3$N$_4$ into TiO$_2$ was optimal, as it resulted in a higher crystallite size and crystallinity index. This finding aligns with previous research suggesting that the hydrothermal synthesis method impacts crystallinity due to the application of high temperature and pressure to the precursors [22].

$$\text{Scherrer equation, } L = \frac{K\lambda}{\beta} . \cos\theta \qquad \text{Eqn. 1}$$

Table 1. Crystallite size and crystallinity index of synthesized photocatalysts.

Sample	TiO$_2$	g – C$_3$N$_4$	TCN$_1$	TCN$_2$	TCN$_5$	TCN$_{10}$
Crystallite size (nm)	6.92	6.27	6.92	6.92	6.97	6.92
Crystallinity index (%)	65.02	65.32	56.37	63.21	72.62	45.58

114 Nur Aien Muhamad, Muhamad Afiq Rosli, Siti Raihan Hamzah, Nureel Imanina Abdul Ghani, Nadiah Sabihah Md Natar, Mohammad Saifulddin Mohd Azami, Mohd Azlan Mohd Ishak, Sumiyyah Sabar and Wan Izhan Nawawi Wan Ismail

Aqua-Mediated Hydrothermal Synthesis in the Production of a g-C$_3$N$_4$/TiO$_2$ Composite for Photocatalytic Degradation of RR4 Dye
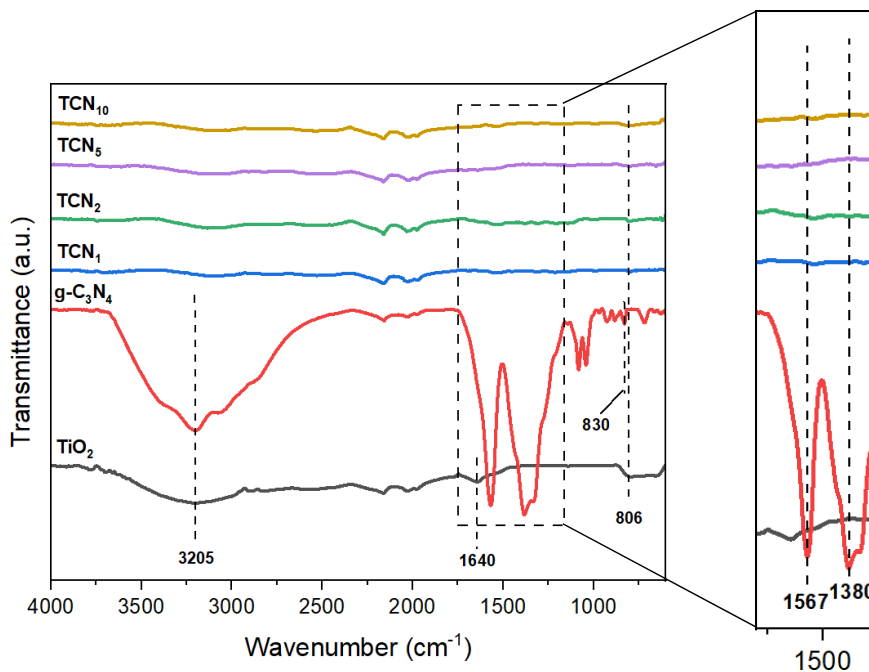
Figure 4. FTIR spectra of TiO$_2$, g-C$_3$N$_4$, TCN$_1$, TCN$_2$, TCN$_5$ and TCN$_{10}$.
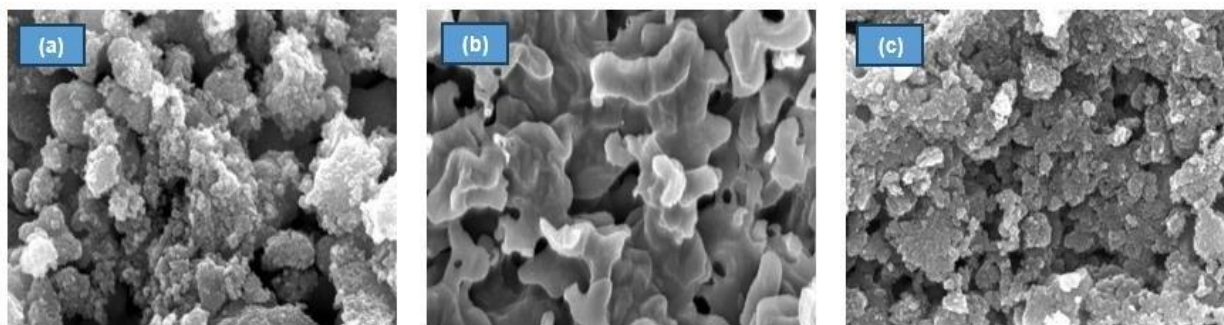
Figure 5. FESEM images of (a) TiO$_2$, (b) g-C$_3$N$_4$ and (c) TCN$_5$.

As the g-C$_3$N$_4$ peak remains undetectable in the TCN$_X$ sample for XRD analysis, additional characterization was conducted using FTIR to examine the molecular structure of the synthesized samples. **Figure 4** illustrates the FTIR spectra of g-C$_3$N$_4$, TiO$_2$, and the g-C$_3$N$_4$/TiO$_2$ composite. In the TiO$_2$ spectrum, distinct peaks at 806 cm^{-1} and 1640 cm^{-1} corresponded to Ti-O and Ti-OH bonds, respectively [23]. Furthermore, a broad peak was observed at 3205 cm^{-1}, indicative of the presence of the O-H bond due to moisture. In pure g-C$_3$N$_4$, the absorption band at 830 cm^{-1} was identified as the triazine peak, while the prominent peaks at 1380 cm^{-1} and 1567 cm^{-1} corresponded to the stretching of aromatic C-N bonds. Additionally, the broad peak at 3205 cm^{-1} indicated the presence of N-H and N-H$_2$ bonds [24]. In the g-C$_3$N$_4$/TiO$_2$ spectrum, the peaks resembled those of the synthesized g-C$_3$N$_4$ and TiO$_2$. However, the intensity of the g-C$_3$N$_4$ peaks was reduced, primarily due to the limited quantity of g-C$_3$N$_4$ in the TiO$_2$ composite.

Surface characteristics of the composite material, comprising g-C$_3$N$_4$, TiO$_2$, and TCN$_5$, were examined using FESEM analysis. **Figure 5** displays the FESEM images, illustrating that the g-C$_3$N$_4$, synthesized from urea, displayed a layered, laminar-like structure [25]. In contrast, TiO$_2$ exhibited a spherical structure with a consistent size distribution [26], as depicted in **Figure 5(a)**. The surface of g-C$_3$N$_4$ appeared to consist of stacked layers, while TiO$_2$ exhibited a uniform, round shape. When conducting FESEM analysis on the TCN$_5$ sample, it became evident that TiO$_2$ was clearly present, whereas the g-C$_3$N$_4$ component was not visually discernible. This can be attributed to the relatively low proportion of g-C$_3$N$_4$ within the composite material.
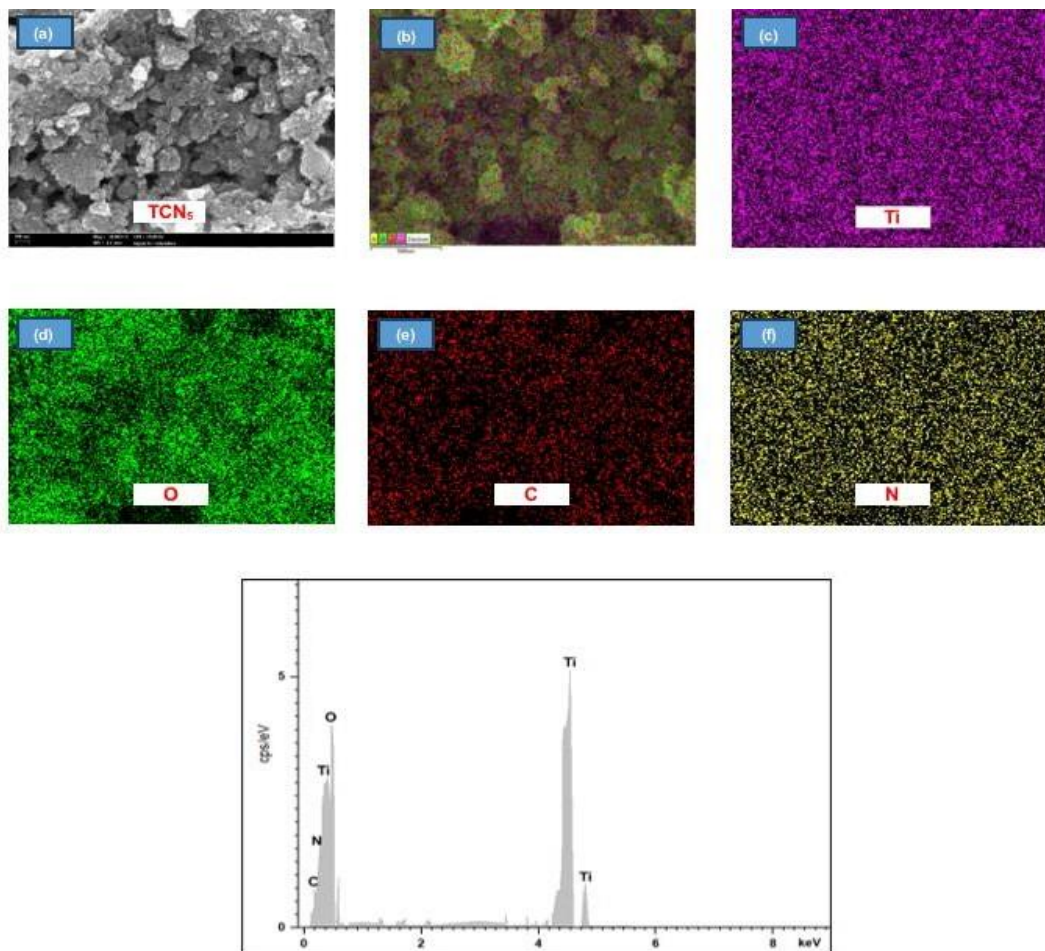
115 Nur Aien Muhamad, Muhamad Afiq Rosli, Siti Raihan Hamzah, Nureel Imanina Abdul Ghani, Nadiah Sabihah Md Natar, Mohammad Saifulddin Mohd Azami, Mohd Azlan Mohd Ishak, Sumiyyah Sabar and Wan Izhan Nawawi Wan Ismail

Aqua-Mediated Hydrothermal Synthesis in the Production of a g-C$_3$N$_4$/TiO$_2$ Composite for Photocatalytic Degradation of RR4 Dye

Figure 6. (a) FESEM images of TCN$_5$, elemental mapping images of (b) TCN$_5$, (c) Ti, (d) O, (e) C, (f) N and (g) EDX analysis of TCN$_5$.

Hence, a comparison of particle sizes was conducted to differentiate between TiO$_2$ and TCN$_5$. TiO$_2$ exhibited a particle size of 31.03 nm, and upon forming a composite with g-C$_3$N$_4$, the particle size decreased to 21.08 nm. To affirm the presence of g-C$_3$N$_4$ in the composite material, elemental mapping was employed. This analysis was conducted to validate the distribution of elements within the TCN$_5$ sample, as shown in **Figure 6**. According to **Figure 6(c-f)**, Ti, O, N and C and were present in the synthesized photocatalyst, providing strong evidence that g-C$_3$N$_4$ had been successfully composited into the TiO$_2$ matrix. However, the concentration of C and N was still low, demonstrating that only a small quantity of g-C$_3$N$_4$ was incorporated into TiO$_2$, as shown in **Figure 6(b).** Therefore, an EDX analysis was performed to determine the atomic weight percentages, which are illustrated in **Figure 6(g)**. The atomic weight percentages of Ti, O, C and N, in g-C$_3$N$_4$/TiO$_2$, were found to be 69.75 %, 11.36 %, 14.17 %, and 4.72 %, respectively.

Figure 7 presents the UV–Vis DRS which was performed to study the optical properties of the sample

and to provide an insight into the light-absorption capabilities of TiO$_2$, g-C$_3$N$_4$, and the TCN$_5$ composite [27]. In **Figure 7(a)**, the absorption wavelength of g-C$_3$N$_4$ extended to 420 nm, while absorption of TiO$_2$ was limited to wavelengths below 390 nm. This indicates that pure TiO$_2$ was only responsive to ultraviolet (UV) light, while g-C$_3$N$_4$ was in the visible light region [28]. In order to determine the bandgap energy of the synthesized photocatalyst, the Tauc equation was used, as follows:

$$(\alpha h v)^n = A(h v - E_g) \qquad \text{Eqn. 2}$$

where α, h, v, E_g, n, and A are the absorption coefficient, Planck's constant, frequency of light, band gap energy of the materials, and constants, respectively [299]. Following the use of the Tauc equation, a Kubelka-Munk function plot, as shown in **Figure 7(b)**, was constructed to determine the bandgap energy of the photocatalysts, and it showed that the band gap energies of TiO$_2$, g-C$_3$N$_4$ and TCN$_5$ were 3.2 eV, 2.7 eV and 3.07 eV, respectively. The observed reduction in the bandgap energy of TCN$_5$ may be attributed to the presence of g-C$_3$N$_4$, which

116 Nur Aien Muhamad, Muhamad Afiq Rosli, Siti Raihan Hamzah, Nureel Imanina Abdul Ghani, Nadiah Sabihah Md Natar, Mohammad Saifulddin Mohd Azami, Mohd Azlan Mohd Ishak, Sumiyyah Sabar and Wan Izhan Nawawi Wan Ismail

Aqua-Mediated Hydrothermal Synthesis in the Production of a g-C$_3$N$_4$/TiO$_2$ Composite for Photocatalytic Degradation of RR4 Dye

enhances interfacial electron transfer and, consequently, promotes efficient spatial separation of photogenerated electron-hole pairs within g-C$_3$N$_4$ [30]. These results confirm that the formation of a heterojunction between g-C$_3$N$_4$ and TiO$_2$ could narrow the bandgap of TiO$_2$ and enhance visible light availability.
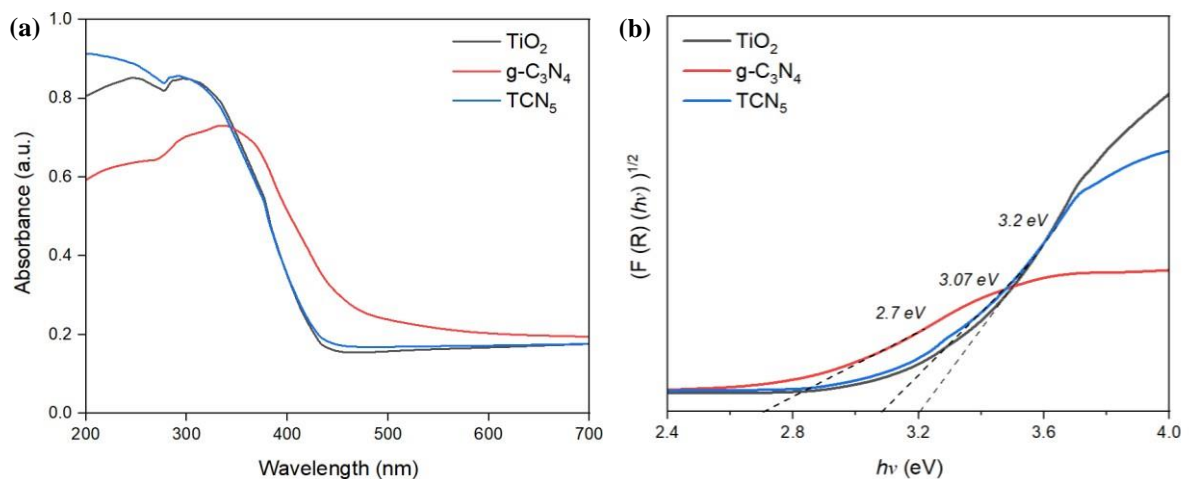

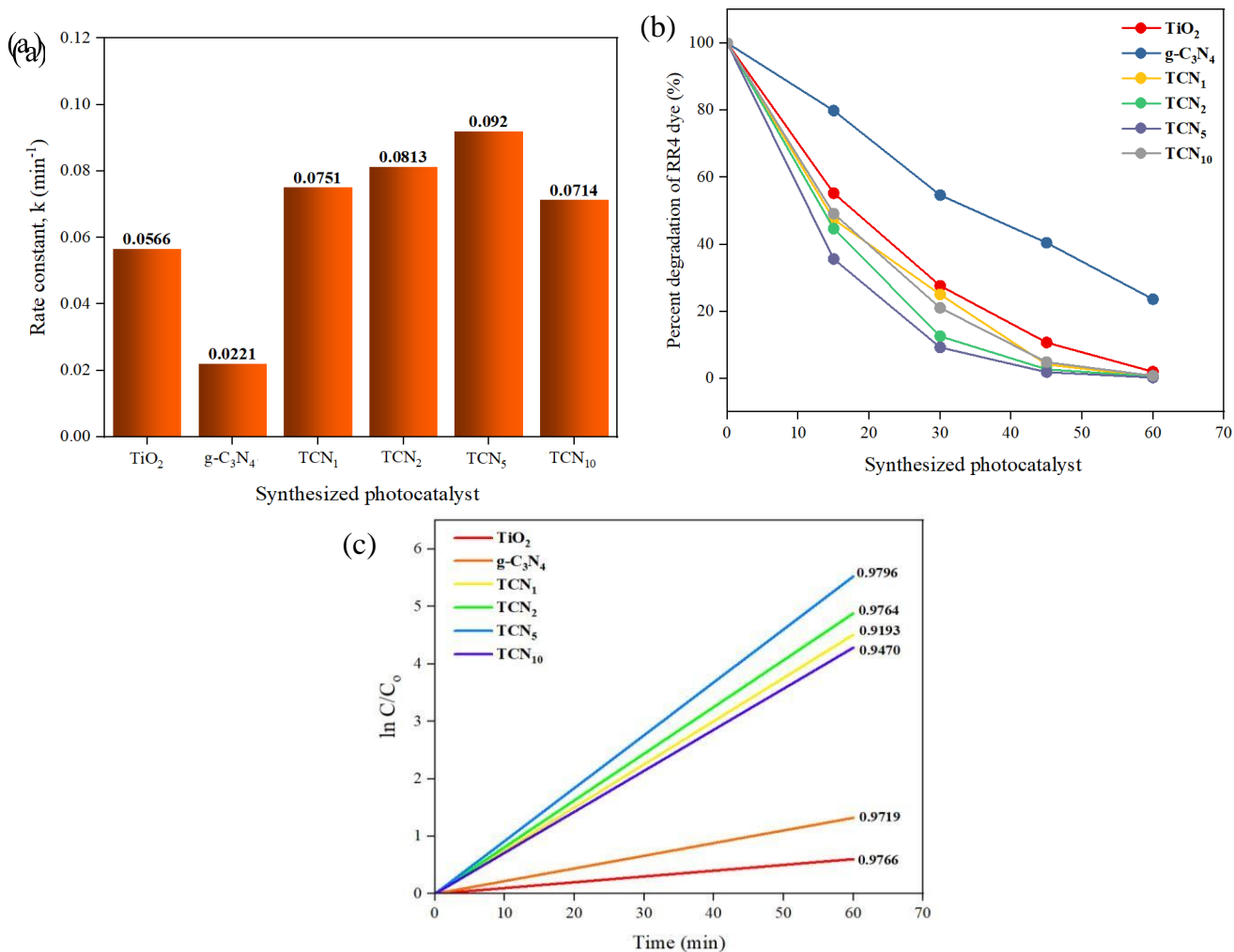**Figure 7**. (a) UV-Vis DRS spectrum and (b) Kubelka-Munk function of synthesized sample.

Figure 8. (a) Rate constant, k (b) percentage removal and (c) plot of ln C/Co vs1-hour degradation of RR4 dye using TiO$_2$, g-C$_3$N$_4$, TCN$_1$, TCN$_2$, TCN$_5$ and TCN$_{10}$.
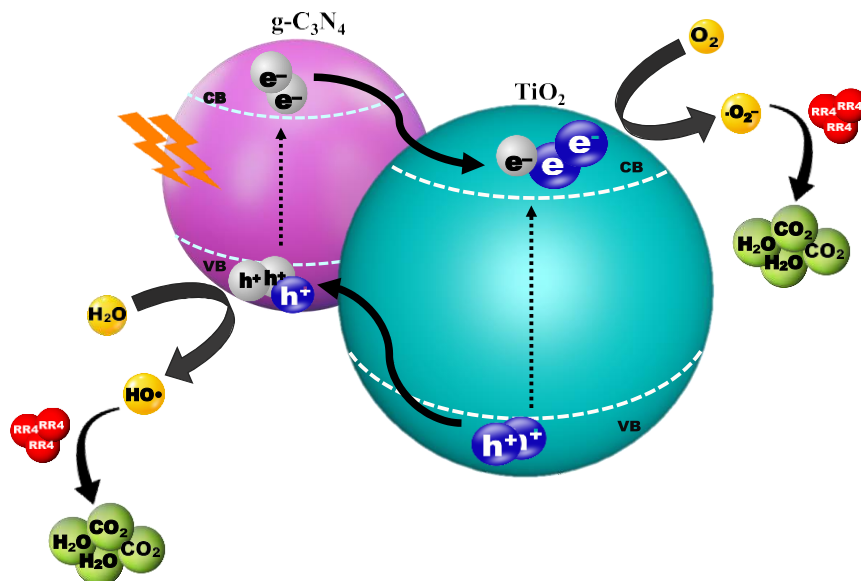
117 Nur Aien Muhamad, Muhamad Afiq Rosli, Siti Raihan Hamzah, Nureel Imanina Abdul Ghani, Nadiah Sabihah Md Natar, Mohammad Saifulddin Mohd Azami, Mohd Azlan Mohd Ishak, Sumiyyah Sabar and Wan Izhan Nawawi Wan Ismail

Aqua-Mediated Hydrothermal Synthesis in the Production of a g-C₃N₄/TiO₂ Composite for Photocatalytic Degradation of RR4 Dye

Figure 9. The suggested photocatalytic mechanism of TCN_5 involves a type II heterojunction for degrading RR4 dye within the visible light spectrum.

In **Figure 8(a)** of the study, the rate constants, k of the synthesized photocatalysts for the degradation of RR4 dye are depicted. TCN_5 exhibited a higher rate constant of 0.0920 min^{-1}, whereas TiO_2 and $g-C_3N_4$ had rate constants of 0.0566 min^{-1} and 0.0221 min^{-1}, respectively. This indicates that the TCN_5 performance was 4.16 and 1.67 times more efficient than $g-C_3N_4$/TiO_2. **Figure 8(b)** of the study predominantly focuses on the reaction kinetics of the photocatalytic degradation of RR4 dye, with the experimental data analyzed using a first-order linear equation. **Figure 8(c)** illustrates the photocatalytic performance of TiO_2, $g-C_3N_4$, TCN_1, TCN_2, TCN_5, and TCN_{10} samples under visible light exposure. TiO_2 demonstrated superior photocatalytic activity compared to $g-C_3N_4$, which exhibited the lowest activity for RR4 dye degradation. Notably, the $g-C_3N_4$/TiO_2 composite material was significantly more effective at breaking down RR4 dye than either $g-C_3N_4$ or TiO_2 individually. This suggests that the combination of the two semiconductors generated a synergistic effect that enhanced the photocatalytic activity of the composite material. Among the $g-C_3N_4$/TiO_2 composites, TCN_5 displayed the highest efficiency, with a removal rate of 99.73 %. In comparison, TCN_1, TCN_2, and TCN_{10} exhibited lower removal rates at 99.44 %, 99.45 %, and 99.19 %, respectively.

Proposed Mechanism

The photocatalytic mechanism of TCN_5 for the degradation of RR4 dye under visible light conditions is explained in **Figure 9**. The proposed mechanism is a type II heterojunction, a structural arrangement that plays a crucial role in improving photocatalytic

activity by reducing the recombination of electrons and holes, thus facilitating the generation of more radicals [31]. The electrons, e^- transition from the valence band (VB) to the conduction band (CB) of TiO_2 after light has penetrated, resulting in an excess of holes, h^+ in the VB of the TiO_2. The e^- from the CB of TiO_2 migrate to the VB of $g-C_3N_4$ where they can participate in the redox reaction process. This electron transfer process is facilitated by the energy level alignment between the TiO_2 and $g-C_3N_4$, which allows for efficient charge separation and transfer at the heterojunction interface. This leads to the generation of radicals, which may act as destroyers of organic pollutants in wastewater [32]. In this study, formation of powerful oxidizing agents (•OH radicals) led to the breakdown of the RR4 dye molecules, and production of the harmless substances, CO_2 and H_2O.

CONCLUSION

We successfully prepared the $g-C_3N_4$/TiO_2 composite using water as a solvent, employing a straightforward sol-gel and hydrothermal approach. We confirmed the synthesis through various characterization analyses, including XRD, where all synthesized samples exhibited discernible peaks. Notably, the TiO_2 synthesized in our study displayed a peak matching that of commercially available TiO_2, confirming its anatase phase. As the $g-C_3N_4$ peak was not clearly observed in the TCN_X sample due to its low weight percentage when combined with TiO_2, we conducted additional analyses such as FTIR, FESEM and mapping to verify the presence of $g-C_3N_4$ in the TCN_X sample. The photocatalytic performance of our synthesized sample was assessed by evaluating its ability to degrade

118 Nur Aien Muhamad, Muhamad Afiq Rosli, Siti Raihan Hamzah, Nureel Imanina Abdul Ghani, Nadiah Sabihah Md Natar, Mohammad Saifulddin Mohd Azami, Mohd Azlan Mohd Ishak, Sumiyyah Sabar and Wan Izhan Nawawi Wan Ismail

Aqua-Mediated Hydrothermal Synthesis in the Production of a g-C₃N₄/TiO₂ Composite for Photocatalytic Degradation of RR4 Dye

RR4 dye. Among the various composite samples synthesized, TCN_5 demonstrated exceptional efficiency, achieving a degradation rate of 99.73%. This surpassed the performance of both the synthesized TiO_2 and pure $g-C_3N_4$. Consequently, our findings suggest that the use of the $g-C_3N_4/TiO_2$ composite is an efficient approach for RR4 dye degradation and holds significant promise for effective environmental remediation applications.

DECLARATION OF COMPETING INTEREST

The authors declare that they have no known competing financial interests or personal relationships that could have appeared to influence the work reported in this paper.

ACKNOWLEDGEMENTS

REFERENCES

1. Al-Tohamy, R., Ali, S. S., Li, F., Okasha, K. M., Mahmoud, Y. A. G., Elsamahy, T. & Sun, J. (2022) A critical review on the treatment of dye-containing wastewater: Ecotoxicological and health concerns of textile dyes and possible remediation approaches for environmental safety. *Ecotoxicology and Environmental Safety*, **231**, 113160.

2. Alsukaibi, A. K. (2022) Various approaches for the detoxification of toxic dyes in wastewater. *Processes*, 10(10), 1968.

3. Abdullah, F. H., Bakar, N. A. & Bakar, M. A. (2022) Current advancements on the fabrication, modification, and industrial application of zinc oxide as photocatalyst in the removal of organic and inorganic contaminants in aquatic systems. *Journal of hazardous materials*, **424**, 127416.

4. Guo, Q., Zhou, C., Ma, Z. & Yang, X. (2019) Fundamentals of TiOF photocatalysis: concepts, mechanisms, and challenges. *Advanced Materials*, **31(50)**, 1901997.

5. DiMeglio, J. L., Breuhaus-Alvarez, A. G., Li, S. & Bartlett, B. M. (2019) Nitrate-mediated alcohol oxidation on cadmium sulfide photocatalysts. *ACS Catalysis*, **9(6)**, 5732−5741.

6. Wan Ismail, W. I. N., Ain, S. K., Zaharudin, R., Jawad, A. H., Ishak, M. A. M., Ismail, K. & Sahid, S. (2015) New TiO₂/DSAT immobilization system for photodegradation of anionic and cationic dyes. *International Journal of Photoenergy*, **2015**.

7. ul Haq, A., Saeed, M., Khan, S. G. & Ibrahim, M. (2021) Photocatalytic applications of titanium dioxide (TiO₂). *Titanium Dioxide-Advances and Applications*.

8. Ibrahim, N. S., Leaw, W. L., Mohamad, D., Alias, S. H. & Nur, H. (2020) A critical review of metal-doped TiO₂ and its structure–physical properties–photocatalytic activity relationship in hydrogen production. *International Journal of Hydrogen Energy*, **45(53)**, 28553−28565.

9. Patil, S. B., Basavarajappa, P. S., Ganganagappa, N., Jyothi, M. S., Raghu, A. V. & Reddy, K. R. (2019) Recent advances in non-metals-doped TiO₂ nanostructured photocatalysts for visible-light driven hydrogen production, CO2 reduction and air purification. *International Journal of Hydrogen Energy*, **44(26)**, 13022−13039.

10. Meng, A., Zhang, L., Cheng, B. & Yu, J. (2019) Dual cocatalysts in TiO₂ photocatalysis. *Advanced Materials*, **31(30)**, 1807660.

11. Hayat, A., Al-Sehemi, A. G., El-Nasser, K. S., Taha, T. A., Al-Ghamdi, A. A., Syed, J. A. S. & Nawawi, W. I. (2022) Graphitic carbon nitride (g–C3N4)–based semiconductor as a beneficial candidate in photocatalysis diversity. *International Journal of Hydrogen Energy*, **47(8)**, 5142−5191.

12. Yan, W., Yan, L. & Jing, C. (2019) Impact of doped metals on urea-derived g-C3N4 for photo-catalytic degradation of antibiotics: Structure, photoactivity and degradation mechanisms. *Applied Catalysis B: Environmental*, **244**, 475−485.

13. Aslam, I., Farooq, M. H., Ghani, U., Rizwan, M., Nabi, G., Shahzad, W. & Boddula, R. (2019) Synthesis of novel g-C3N4 microrods: A metal-free visible-light-driven photocatalyst. *Materials Science for Energy Technologies*, **2(3)**, 401−407.

14. Jung, H., Pham, T. T. & Shin, E. W. (2019) Effect of g-C3N4 precursors on the morphological structures of g-C3N4/ZnO composite photo-catalysts. *Journal of Alloys and Compounds*, **788**, 1084−1092.

15. Kumar, S., Battula, V. R. & Kailasam, K. (2021) Single molecular precursors for CxNy Materials-Blending of carbon and nitrogen beyond g-C3N4. *Carbon*, **183**, 332–354.